LANGMUIR Article
Cite This: Langmuir 2019, 35, 3999−4010
pubs.acs.org/Langmuir

Shape and Phase Transitions in a PEGylated Phospholipid System

Lauri Viitala,[†] Saija Pajari,[†] Luigi Gentile,[‡,§,⊥] Jukka Määttä,[†] Marta Gubitosi,[‡] Jan Deska,[†] Maria Sammalkorpi,[†] Ulf Olsson,[‡] and Lasse Murtomäki*[,†]

[†]Department of Chemistry and Materials Science, Aalto University, P.O. Box 16100, FI-00076 Aalto, Finland
[‡]Physical Chemistry, Lund University, P.O. Box 124, SE-221 00 Lund, Sweden
[§]Department of Biology, MEMEG Unit, Lund University, Sölvegatan 37, SE-223 62 Lund, Sweden
[⊥]PRPDepartment of Chemistry, University of Bari Aldo Moro, Via Orabona 4, 70126 Bari, Italy

Supporting Information

ABSTRACT: Poly(ethylene glycol) (PEG) polymers and PEG-conjugated lipids are widely used in bioengineering and drug transport applications. A PEG layer in a drug carrier increases hydrophilic repulsion, inhibits membrane fusion and serum opsonin interactions, and prolongs the storage and circulation time. It can also change the carrier shape and have an influence on many properties related to the content release of the carrier. In this paper, we focus on the physicochemical effects of PEGylation in the lipid bilayer. We introduce laurdanC as a fluorophore for shape recognition and phase transition detection. Together with laurdanC, cryogenic transmission electron microscopy, differential scanning calorimetry, molecular dynamics simulations, and small-angle X-ray scattering/wide-angle X-ray scattering, we acquire information of the particle/bilayer morphology and phase behavior in systems containing 1,2-dipalmitoyl-*sn*-glycero-3-phosphocholine:1,2-distearoyl-*sn*-glycero-3-phosphoethanolamine-PEG(2000) with different fractions. We find that PEGylation leads to two important and potentially usable features of the system. (1) Spherical vesicles present a window of elevated chain-melting temperatures and (2) lipid packing shape-controlled liposome-to-bicelle transition. The first finding is significant for targets requiring multiple release sequences and the second enables tuning the release by composition and the PEG polymer length. Besides drug delivery systems, the findings can be used in other smart soft materials with trigger-polymers as well.

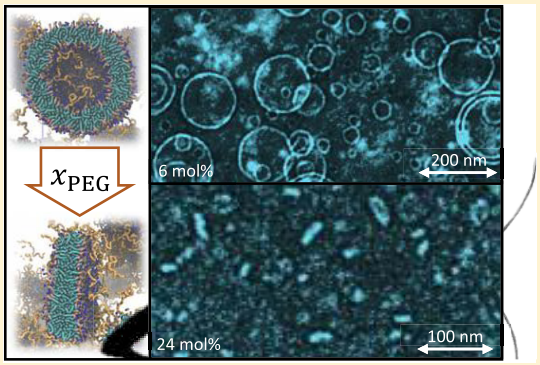

INTRODUCTION

In aqueous solutions, phospholipids form various structures. These include liposomes and micelles. Bicelles are a specific subgroup of micelles. They contain a bilayer and are discoidal in shape. Liposomes are used in drug delivery due to their ability to encapsulate hydrophilic molecules into their aqueous core. The hydrophobic part in the bilayer can also be used since lipophilic molecules have an affinity toward the lipid tails. Hence, liposomes,[1] bicelles,[2] and micelles[3,4] can be used in drug delivery purposes alike. In the most typical scheme, a target cell internalizes a carrier via endocytosis and a hydrophilic drug is released by some internal or external trigger. These include changes in pH,[5] temperature,[6] or radiation in the ultraviolet,[7,8] visible,[9,10] or near infrared[9,11−14] region. Here, the trigger is set to alter the phase order in the lipid bilayer, resulting in an increased permeation and release of the drug[14,15] or any encapsulated cargo.[16]

Drug delivery systems face many obstacles as they pass through the hostile environments of epithelia. Unfortunately, liposomes are usually targeted by serum opsonin and opsonized liposomes are removed from the circulation by specialized phagocytic cells in a matter of hours.[17,18] Surviving this clearance is a major objective, because a longer circulation time increases chances of reaching the target cell. Opsonin targeting can be prevented by adding poly(ethylene glycol) (PEG) moieties on the surface of the carrier, usually at the concentration of ca. 5 mol %, which is a procedure sometimes portrayed as "the gold standard".[19,20] The PEG layer adds a steric barrier against opsonins and other bioactive molecules.[21] It increases circulation time and provides a stealth sheath that stabilizes the drug delivery system in blood and in storage. A good example of this approach is Doxil (a liposomal drug formulation that is used to deliver chemotherapeutic doxorubicin into the cancer cells). Doxil was approved by the FDA in 1995.[22]

In addition to the steric barrier, PEG changes the extent of hydration of the bilayer[23] and inhibits its interaction with divalent ions, most commonly Ca^{2+}, decreasing the extent of membrane fusion.[24,25] Interestingly, PEG can be solubilized in both hydrophilic and hydrophobic solvents.[26] Hence, it can be used to bind not only the hydrophilic molecules, like albumin,[27,28] but also more hydrophobic molecules, e.g.,

Received: November 14, 2018
Revised: February 18, 2019
Published: February 21, 2019

DOI: 10.1021/acs.langmuir.8b03829
Langmuir 2019, 35, 3999−4010

indocyanine green.[12,29] Due to its hydrophobic moieties, it has been hypothesized that PEG may even partly penetrate into the liquid crystal or fluid phase of the bilayer found at high temperatures.[25] This obviously affects the behavior of a lipid system as a drug carrier and releaser.

PEG has been studied experimentally and computationally. In coarse-grained molecular dynamics (MD) simulations, transferable PEG models have been introduced by Lee et al.,[30] Rossi et al.,[31] and Grunewald et al.[32] These models have been utilized in simulations of PEGylated lipid bilayers and lipid aggregates.[25,33−38] Experimentally, PEGylation has been shown to not only affect the phase transition behavior of the lipid systems,[39] but also the particle shape. The latter was also obtained in simulations by Lee and Pastor.[33]

The shape of the lipid aggregate depends on its lipids. For example, pure 1,2-dipalmitoyl-*sn*-glycero-3-phosphocholine (DPPC) and 1,2-distearoyl-*sn*-glycero-3-phosphocholine (DSPC) form liposomes and pure PEG-terminated 1,2-distearoyl-*sn*-glycero-3-phosphoethanolamine (DSPE-PEG) forms globular micelles, but with sufficient PEGylation they both form bicelles.[40−43] Similarly, L-α-phosphatidylcholine (EPC) forms liposomes but the EPC:DSPE-PEG system forms long cylindrical micelles instead of bicelles.[40,41,43,44] The shape is usually predicted by the spontaneous curvature[45−48] (or the packing parameter[49,50]) of the lipid or the lipid mixture. This parameter is characteristic of a single lipid, and DPPC and EPC are not actually much different in this aspect. Segregation of the lipids can cause the formation of bicelles, whereas a nonsegregated lipid system (i.e., EPC system) form long cylindrical micelles.[51] The rigidity of the bilayer plays a key role[52] because it affects the segregation of lipids. For instance, EPC:DSPE-PEG with cholesterol (40 mol %) forms bicelles due to the stiffening of the tail groups.[40,43]

In this paper, we have studied the physicochemical effects of PEGylation on the structure, shape, and sizes of the lipid systems containing DPPC and DSPE-*N*-[amino(poly(ethylene glycol))-2000] (DSPE-PEG(2000)). We introduce a new method for the shape recognition using fluorescence emissions of laurdanC. This method is presented along with several other techniques, including new MD simulations that provide a pervasive view on the two effects of PEGylation. The first effect is the shift in the phase transition temperature, measured with differential scanning calorimetry (DSC) and laurdanC. This shift could be utilized in partial drug release with, e.g., photothermal agents,[14] since the most effective drug release occurs in the phase transition temperature region. The transformation from liposomes to bicelles is another effect of PEGylation. Here, we show that laurdanC data correlates with the average aspect ratio of the particles obtained with cryogenic transmission electron microscopy (cryo-TEM). In this way, we have determined the shape transformation threshold at 9.6 mol %, which is also corroborated with MD simulations and small-angle X-ray scattering (SAXS) analysis. Particle sizes from SAXS analysis agree with cryo-TEM images and show with MD simulations that PEGylated lipids are relocated to higher curvature regions. Hence, laurdanC measurements combined with cryo-TEM, SAXS/wide-angle X-ray scattering (WAXS), and MD simulations show that bicelles are formed when the spontaneous curvature of the mixture enables the formation of bicelle rims. This is demonstrated here for DSPE-PEG(2000), but as the findings relate particle shape directly with the polymer packing, they are generalizable to polymer−lipid systems and could be used to design, e.g., drug delivery systems.

MATERIALS AND METHODS

Materials. 1,2-Dipalmitoyl-*sn*-glycero-3-phosphocholine (DPPC) and 1,2-distearoyl-*sn*-glycero-3-phosphoethanolamine-*N*-[methoxy-(poly(ethylene glycol))-2000] (DSPE-PEG(2000)) were purchased from Avanti Polar lipids. Ethanol was purchased from Altia. Carboxylated laurdan (laurdanC) was synthesized using the pathway described by Cheniour et al.[53] with minor changes. Rest of the chemicals were purchased from Sigma-Aldrich unless otherwise stated.

Preparation of Lipid Samples. Samples containing laurdanC were prepared according to ref 14 but using *N*-(2-hydroxyethyl)-piperazine-*N*′-ethanesulfonic acid (HEPES) buffer (150 mM NaCl, 20 mM HEPES in pH 7.4) instead of Tris−HCl. Other samples were prepared as follows: 20 μmol of lipids in chloroform, containing 0, 3, 6, 9, 12, 15, or 24 mol % of DSPE-PEG(2000) were added to a round flask. Chloroform was evaporated in a nitrogen stream and the remaining lipid film was heated up to 60 °C prior to the addition of 2 mL of HEPES buffer. The dispersion was sonicated in a 60 °C bath sonicator for the duration of adding the buffer solution ($\leq$45 s). After this, the dispersion was extruded eleven times through double-stacked polycarbonate membranes with the pore size of 200 nm. The temperature in both steps was constant, at 60 °C. After the extrusion, samples were stored in a refrigerator overnight before further studies.

Cryo-TEM. Vitrified lipid samples were prepared in FEI Vitrobot (FEI) after Kuntsche et al.[54] and Iancu et al.[55] Briefly, ethane gas was condensed halfway into a liquid-nitrogen-cooled Vitrobot cup following liquefaction of propane gas and resulting in a liquefied gas mixture of 1:1 ethane:propane. A plasma-treated (30 s H_2−O_2, Gatan Solarus 950, Gatan) QUANTIFOIL R 2/2 (or R 2/1) copper TEM grid (Electron Microscopy Sciences) was placed inside the Vitrobot chamber and the humidity was increased to 100% at 22 °C. 5 μL of the sample was pipetted onto the TEM grid, the grid was blotted with a filter paper for 1 s, and immersed into the ethane−propane mixture. The grid was then moved into the cryo-TEM sample holder under liquid nitrogen. Micrographs were taken with an FEI Tecnai T12 (FEI) transmission electron microscope (TEM) with 120 kV accelerating voltage.

The size distribution and the number of distinctive particles were determined with a self-made Matlab script (Supporting Information). Each particle type was classified to groups of "liposomal", "bicellar edge" (bicelle edge toward the microscope), "bicellar face" (bicelle face toward the microscope), and "unknown" (irregular shapes) structures. Structures at the vicinity of 5 nm in diameter were excluded from the image analyses since they are difficult to distinguish from the background. The number fraction of bicelles $x_{\text{bicelle}}^{\text{TEM,num}}$ was determined from the number of bicellar shapes vs the total number of particles. However, the signal intensity in, e.g., SAXS, DSC, and dynamic light scattering does not follow the number of particles but the number and the molar mass of monomers in the particles. The number of surfactant molecules is related to the surface area of the particles. Hence, the monomeric bicelle fraction can be determined as

$$x_{\text{bicelle}}^{\text{TEM}} = \frac{N_{\text{bicelle}}}{N_{\text{bicelle}} + \tau N_{\text{liposome}}} \tag{1}$$

where τ is the area-scaling factor. It is a function of the average area of liposomes and bicelles

$$\tau = \frac{\langle A_{\text{liposome}} \rangle}{\langle A_{\text{bicelle}} \rangle} = 4\frac{\langle r_{\text{liposome}} \rangle^2 + (\langle r_{\text{liposome}} \rangle - d)^2}{2\langle r_{\text{bicelle}} \rangle^2 + \pi \langle r_{\text{bicelle}} \rangle d + d^2} \tag{2}$$

where d is the thickness of the bilayer, and r_{liposome} and r_{bicelle} are the average radii of the corresponding particle.

Differential Scanning Calorimetry and Fluorescence Spectroscopy. DSC thermograms were measured with a MicroCal VP-DSC calorimeter (MicroCal Inc., Northampton, MA) between 10 and 60 °C, starting at 10 °C. Heating and cooling rates were 1 and 0.5 °C

DOI: 10.1021/acs.langmuir.8b03829
Langmuir 2019, 35, 3999−4010

min^{-1}, respectively, to obtain similar peak positions and shapes, considering the differences in the phase separation kinetics. Both scan directions were measured twice to ensure the reversibility of the system.

LaurdanC measurements were performed with a PerkinElmer LS5 fluorescence spectrometer in a temperature controlled four-window cuvette. Each measurement was started after stabilization for 3 min at the given temperature between 25 and 70 °C. Smaller temperature intervals (0.5 °C) were used near the phase transition region (i.e., 34−45 °C). The lipid order was calculated with the laurdan generalized polarization (GP)

$$GP = \frac{I_o - I_d}{I_o + I_d} \tag{3}$$

where I_o and I_d represent the emission intensities at the wavelengths corresponding to the ordered (λ_{em} = 430 nm) and disordered state (λ_{em} = 510 nm) of the lipid bilayer. In addition to GP, the derivative $\partial GP/\partial T$ was determined to portray the data similar to the DSC results.

The deconvolution of the DSC data and $\partial GP/\partial T$ peaks was calculated using the Voigt profile analysis package by Ruzi,[56] using a Faddeeva function algorithm.[57] The Matlab script fits multiple Voigt profiles, i.e., the convolution of Gaussian distribution and Cauchy−Lorentz distribution, simultaneously. The number of fitted Voigt profiles was set to 7 in DSC data and 5 in the GP differentials. Signals that were clearly part of the baseline, had zero intensity, or were part of the pre-phase transition were subtracted. Typically, the DSC fits found 3 distinctive Voigt profiles below the main phase transition peaks in DSC but, e.g., the PEG9[a] sample contained 5 distributions in the upward scan and 4 distributions in the downward scan. The peaks were labeled in the order of their position and compared with the like measurement (e.g., downward scan of PEG9 with the other downward scans).

Small/Wide-Angle X-ray Scattering. The SAXS/WAXS measurements were performed using a SAXSLab Ganesha 300XL instrument (SAXSLAB ApS, Skovlunde, Denmark), a pinhole collimated system equipped with a Genix 3D X-ray source (Xenocs SA, Sassenage, France). The scattered intensity was recorded with the detector placed at three sample-to-detector distances yielding a range of the scattering vector q of 0.05−20.0 nm^{-1}. The samples were sealed in a 1.5 mm diameter quartz capillary (Hilgenberg GmbH, Malsfeld, Germany), and the measurements were performed at 25, 41, and 50 °C. In all cases, the temperature was controlled with water circulation with an accuracy of 0.2 °C. The two-dimensional scattering pattern was recorded by using a two-dimensional 300 K Pilatus detector (Dectris Ltd., Baden, Switzerland) and the radial averaging to obtain $I(q)$ was performed with SAXSGui software. The measured scattering curves were corrected for solvent scattering.

The following analyses for the SAXS data were derived following refs 58−65. The total scattering cross-sections are the sum of the liposome and bicelle scattering (i.e., $I_{bicelle}$ and $I_{liposome}$)

$$I_{fit} = x_{bicelles} I_{bicelle} + (1 - x_{bicelles}) I_{liposome} \tag{4}$$

where the fraction of bicelles $x_{bicelles}$ was determined with cryo-TEM. In this form, we assume no interaction between particles. The starting point of $I_{bicelle}$ and $I_{liposome}$ is the corresponding core−shell structure. These are detailed in Supporting Information. Briefly, the form factor of the liposome is

$$P_{s,liposome} = \sum_j \Gamma_j f_{i,j}^{\ 2} \text{ with } f_{i,j} = \sum_i^4 \Delta\rho_i V_{i,j} 3 \frac{\sin qr_{i,j} - qr_{i,j} \cos qr_{i,j}}{(qr_{i,j})^3} \tag{5}$$

where each component layer follows the Rayleigh form factor amplitude,[66] $\Delta\rho_i = \rho_{i-1} - \rho_i$ is the scattering length contrast between the component layers, $r_{i,j}$ is the radius, and $V_{i,j}$ is the volume of the component layer, which is deflected as a function of the polydispersity index (see the Supporting Information). For the bicelle, the form factor is[67]

$$P_{s,bicelle} = \int \sum_j \Gamma_j f_{b,j}^2 \sin\alpha \, d\alpha \text{ with}$$

$$f_{b,j} = \sum_i^4 \Delta\rho_i V_{i,j} \frac{J_1(qr_{i,j} \sin\alpha)\sin(ql_i \cos\alpha)}{q^2 r_{i,j} l_i \sin\alpha \cos\alpha} \tag{6}$$

where each component layer follows cylindrical symmetry according to Fournet,[67] α is the angle between the incident beam and the cylinder normal, J_1 is the modified Bessel function of order 1, and l_i is the half-thickness of the component layer. When the particle surface is covered with PEG, the total scattering cross-section is given as[44,58]

$$I_{tot} = n(P_s + N_c[P_c + 2P_{sc} + (N_c - 1)P_{cc}]) \tag{7}$$

where, in the order of appearance, P_s and P_c are the self-correlation terms of the lipid core and the PEG chain, respectively, P_{sc} and P_{cc} are the cross-correlation terms of the core-chain and the chain−chain interactions, respectively, n is the macroscopic number density of the particles, and N_c is the number of polymer chains on a single particle. Since PEG is essentially a Gaussian random coil with the characteristics detailed by Hammouda,[68,69] the self-correlation term is the well-known Debye function[70]

$$P_c = 2(\Delta\rho_{PEG}^{w} \nu_{PEG})^2 (\exp[-(qR_G)^2] + (qR_G)^2 - 1)(qR_G)^{-4} \tag{8}$$

where $\Delta\rho_{PEG}^{W} = \rho_{PEG} - \rho_0$ is the scattering length density contrast of the PEG chain, ν_{PEG} is the partial specific molecular volume of PEG, and R_G is its radius of gyration. The form factor amplitude times $\Delta\rho_{PEG}^{W} V_{PEG}$ is given as[68,69]

$$f_c = \Delta\rho_{PEG}^{w} V_{PEG} (1 - \exp[-(qR_G)^2])(qR_G)^{-2} \tag{9}$$

There is some irregularity in the presentation of f_c in the literature. Most authors (e.g., refs 58−60 and 65) follow Hammouda,[68,69] but for instance, refs 44 61, and 64 have also used $f_c = \Delta\rho_{PEG}^{W} V_{PEG}(1 - \exp(-qR_G))(qR_G)^{-1}$. The expression $P_c = 2(\Delta\rho_{PEG}^{W} V_{PEG})^2(\exp[-(qR_G)^2] + (qR_G)^2 - 1)(qR_G)^{-2}$ that is found in ref 65 may also cause confusion. Since there should be a general proportionality $P_c \propto f_c^2$, the use of eqs 8 and 9 is well justified since f_c^2, with a Taylor approximation $\exp[-2(qR_G)^2] \approx 1 - 2(qR_G)^2$, results in P_c.

The cross-correlation terms of eq 7 with no azimuth angle dependency can be obtained by combining eqs 5 or 6 with eq 9

$$\begin{cases} P_{sc,k} = f_c \int_{\pi/2}^{0} \sum_j \Gamma_j f_{k,j} \Xi_{k,j} \sin\alpha \, d\alpha \\ P_{cc,k} = f_c^2 \int_{\pi/2}^{0} \sum_j \Gamma_j \Xi_{k,j}^2 \sin\alpha \, d\alpha \end{cases} \tag{10}$$

where $\Xi_{k,j}$ is the form factor amplitude of an infinitely thin shell that connects the polymer with the surface of the underlying core structure.[44] For a liposome with a PEG fraction x_{out} on its outer leaflet and $x_{in} = 1 - x_{out}$ on its inner leaflet

$$\Xi_{l,j} = x_{in} \frac{\sin q(r_{1,j} - R_G)}{q(r_{1,j} - R_G)} + x_{out} \frac{\sin q(r_{4,j} + R_G)}{q(r_{4,j} + R_G)} \tag{11}$$

Since liposomes are relatively large, a good approximation is to let $x_{out} \to 0.5$. In this case, x_{in} and x_{out} can be omitted from eq 11 and the multipliers in eq 7 can be effectively substituted with $N_c \to N_c/2$, which is the approach presented by Arleth et al.[64] The form factor amplitude of a cylindrical shell is[59,61]

$$\Xi_{b,j} = x_{face} \frac{2J_1(qr_{4,j} \sin\alpha)}{qr_{4,j} \sin\alpha} \cos(q(l_4 + R_G)\cos\alpha) + x_{rim} J_0(q(r_{4,j} + R_G)\sin\alpha) \frac{\sin(ql_4 \cos\alpha)}{ql_4 \cos\alpha} \tag{12}$$

where the former term describes the fraction x_{face} of the form factor amplitude with PEG only on the face of the bicelle and the latter

DOI: 10.1021/acs.langmuir.8b03829
Langmuir 2019, 35, 3999−4010

describes the fraction x_{rim} on the rim region. Uniform polymer coating is obtained when $x_{rim,uniform} = 2l_4(r_4 + 2l_4)^{-1}$.[61]

Computational Methods. Molecular dynamics (MD) simulations of pure DPPC and mixtures of DPPC and DSPE-PEG(2000) in water were performed to support the experimental observations. The model used here is based on the implicit-solvent version of the CG MARTINI model,[71,72] called DRY-MARTINI.[73] Similar to the standard MARTINI PEG models,[30,31] a 3-to-1 CG mapping for the PEG is used, whereas the lipids are treated with the 4-to-1 DRY-MARTINI CG mapping scheme. Additional model details are provided in the Supporting Information.

The simulations were run with Gromacs 5.1.1[74] in the NVT ensemble. Temperature was maintained at T = 323 K by the stochastic velocity rescaling thermostat of Bussi et al.[75] with the stochastic friction time constant τ_t = 4.0 ps. The equations of motion were integrated by the second-order stochastic dynamics integrator using a time step of 40 fs. A cut-off of 1.1 nm was used for both the Lennard-Jones (LJ) and electrostatic interactions with the LJ interaction potential shifted to zero at the cut-off. As for the reaction-field electrostatics, relative permittivity ε_r = 15 was used beyond the cut-off distance. In total, the simulation protocol follows the standard DRY-MARTINI protocol[73] augmented by the improved Verlet integration protocol of ref 76.

Following the experimental setup, mixtures of DPPC and DSPE-PEG(2000), i.e., DSPE lipids with 45 CH_2CH_2O monomers, are examined. The structures and the construction of the DSPE-PEG model can be found in our earlier publications.[36,77] Four different molecular compositions were studied. These contained (1) 10 500 DPPC molecules (PEG0), (2) 10 269 DPPC and 231 DSPE-PEG molecules (PEG2.2), (3) 9400 DPPC and 1100 DSPE-PEG molecules (PEG10.5), and (4) 5250 DPPC and 5250 DSPE-PEG molecules (PEG50). Each lipid was also associated with a Na^+ counter-ion to maintain the electroneutrality in the systems. The water interaction in the system is given implicitly by the DRY-MARTINI model.

Initial configurations were constructed by distributing the lipids randomly in the simulation box. The PEG chains were set to an extended coil state. A simulation box of 50 nm × 50 nm × 50 nm was used with PEG0, PEG2.2, and PEG10.5 systems and 100 nm × 100 nm × 100 nm for the PEG50 system. For assessing lipid segregation and bicelle thickness, 30 nm × 30 nm × 30 nm systems of self-assembled single bicelles of size 1050 lipids, with the corresponding DSPE-PEG2000 fractions, were analyzed. All systems were initially energy minimized by using the steepest descent algorithm after which an MD run was performed in the NVT ensemble with the total duration of 0.5 μs.

RESULTS AND DISCUSSION

Microscopic Characteristics of PEGylated lipid systems. Typical cryo-TEM image of the PEG3 and PEG24 samples are shown in Figure 1A,B. In all PEGylated samples, only a few types of particles were observed. These were liposomes (Figure 1C) and bicelles (Figure 1D,E). The PEG24 sample also contained some objects close to the resolution limit of cryo-TEM (5 nm).[78] These particles are difficult to qualify from the background. Hence, they were disregarded. As depicted in refs 40−43, bicelles are typically orientated with their edge (Figure 1D) or their facet (Figure 1E) facing the microscope. Intermediate orientations were also found and counted in as face oriented bicelles. The orientation is influenced by the nearby surface and the thickness of the sample film that is biconcave across the sample hole.[78] Larger liposomes and bicelles with edge orientation prefer the perimeter, where the solvent layer is thicker and the aperture wall closer. Smaller particles, including face orientated bicelles, occupy the center of the image increasingly at $x_{PEG} > 0.12$. In some rare occasions, seemingly saddle-shaped (in PEG12) or

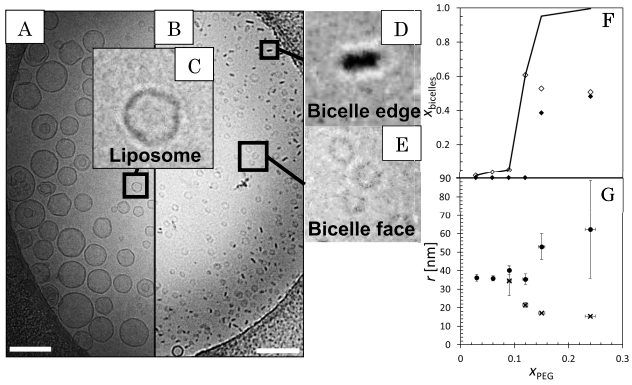

Figure 1. Typical cryo-TEM image of PEG3 (A) and PEG24 (B). Scale bar is 200 nm. (C), (D), and (E) display liposomes, edge bicelles, and face bicelles, respectively. The total fraction and the subset bicelle fraction are depicted in (F) with bicelle face and edge as filled diamonds and unfilled diamonds, respectively. The size of the liposomes (dots) and bicelles (crosses) is shown in (G).

folded bicelles (in PEG9) could be observed. The fractions of the bicellar units are shown in Figure 1F. As can be seen, bicellar units start to emerge rapidly at $x_{PEG} > 0.09$ and bicellar faces appear in the sample with 15 mol % of PEGylation. Thus, the system undergoes a transformation from liposomes to bicelles at ca. 10 mol % and the orientation becomes more random when the bicelle size decreases,[78] which is evident from the cryo-TEM data in Figure 1G. Although the number of bicelles increases, their average size decreases and the size of the remaining liposomes increases. This marks a clear separation between the shapes and it shows that the smallest units have a strong affinity to produce disks.

The SAXS patterns (Figure 2A) of the low PEGylation resembles those of Pili et al.,[79] who measured similar systems with synchrotron-based SAXS. The SAXS data were fitted (red lines) with parameters in Table S1 of the Supporting Information. The particle radius (Figure 2B) was determined as the sum of the core radius and the half of the bilayer thickness (Figure 2C) that increases when DPPC is coupled with longer lipids (i.e., DSPE-PEG). The radii match well with the cryo-TEM results; black line in Figure 2B shows the average radii from Figure 1G.

The radius of gyration R_G showed a gradual increase (Figure 2D) when PEG was added. With low PEGylation (PEG3), the effect of R_G is very small and more accurate estimation is difficult to obtain. At high PEGylation, R_G goes to 1.75 nm and increases to 1.92 nm in samples containing only bicelles. These values are reasonable for PEG with a molar mass of 2 kDa.[80,81]

The location of the polymers was also determined. On PEG3 liposomes, the PEG moieties have no preference, but in PEG6, the proportion (31:69) favors the outer leaflet. In bicelles, the PEG units are more readily found on the edge, as can be seen in Figure 2E, where the ordinate displays the difference between the fitted value and the uniform polymer coating ($x_{rim,uniform} = 2l_4(r_4 + 2l_4)^{-1}$).[61]

The fitting parameters differ slightly from those in the literature. The SANS data of Arleth et al.[64] is equivalent to $\rho_{PEG} = 1.11 \times 10^{11}$ cm^{-2}, $\rho_{tail} = 0.83 \times 10^{11}$ cm^{-2}, and $\rho_{head} = 1.45 \times 10^{11}$ cm^{-2}. Quite close to this, we obtained $\rho_{PEG} = 1.08 \times 10^{11}$ cm^{-2} and $\rho_{tail} = 0.87 \times 10^{11}$ cm^{-2} for liposomes and $\rho_{tail} = 0.85 \times 10^{11}$ cm^{-2} for bicelles. The head group scattering length densities had more variation, stemming partially from the difference of D_2O buffer and water. This is somewhat

DOI: 10.1021/acs.langmuir.8b03829
Langmuir 2019, 35, 3999−4010

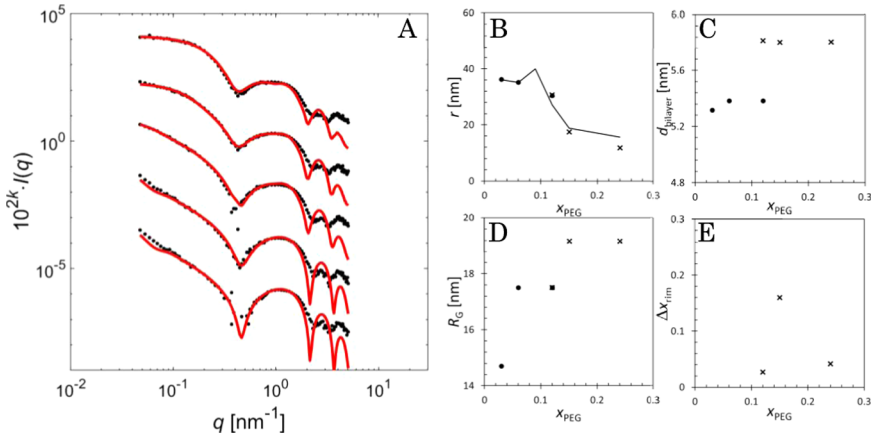

Figure 2. A) SAXS fits (red lines). Black dots represent the SAXS measurements of PEG3 ($k = -2$), PEG6 ($k = -1$), PEG12 ($k = 0$), PEG15 ($k = 1$), and PEG24 ($k = 2$). Fit parameters for liposomes (dots) and bicelles (crosses): (B) radius (the line is the cryo-TEM average), (C) bilayer thickness, (D) radius of gyration of PEG, and (E) excess amount of PEG on the rim region.

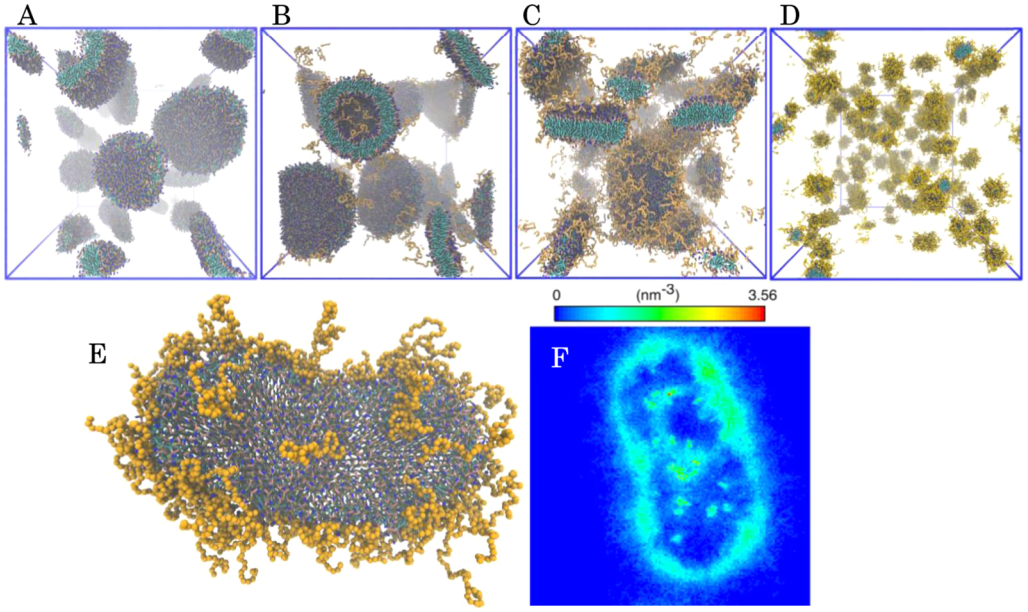

Figure 3. Snapshots of the aggregates in 0.5 μs molecular dynamics simulations. Panel (A) shows pure DPPC, panel (B) DPPC with 2.2 mol % DSPE-PEG, panel (C) DPPC and 10.5 mol % DSPE-PEG, and panel (D) 50 mol % PEGylated lipid. Panel (E) shows a detailed structure of a bicelle of 1050 molecules containing 10.5 mol % DSPE-PEG, and panel (F) is the DSPE lipid density profile of the same bicelle.

expected; Pedersen and Gerstenberg[58] have shown that SAXS measurements of polymer micelles in H_2O cannot be readily fitted with parameters obtained from SANS measurements in D_2O.

The SAXS fits in Figure 2A are accurate in the q range 0.1−2 nm^{-1} for all PEGylated samples, and the fits of PEG12, PEG15, and PEG24 are accurate in the entire lower q range. The intermediate range provides the shape and size of the particles. Thus, the small divergence of the PEG3 and PEG6 fits in the very low q range is not significant, and the presence of spherical and discoid structures is consolidated with SAXS. The radii (Figure 2C) are almost equal to those measured with cryo-TEM (Figure 1G) although the radius of the PEG24 bicelle was smaller than that in the cryo-TEM images. This may result from the appearance of particles smaller than the ones quantified in cryo-TEM.

The fits in Figure 2A deviate from the measurements in the high q range. For simplicity, the fitting function did not contain a constant effective background to account for scattering associated with the internal fluid structure of the bilayer. Thus, the fit decays faster at high q than the experimental data. Nevertheless, the fit clearly captures the form factor oscillations, proving that the thicknesses in Figure 2C are in the correct size range. Yet, the determination of the bilayer thickness may not be accurate because the high q region is susceptible to errors in solvent subtraction and the measured intensities do not fall between the behavior of a centrosymmetric sphere model (q^{-4})[61] and a Gaussian random coil model (q^{-2})[61] in either the liposome or bicelle system.

The shape transformation was also verified with MD simulations in Figure 3. Figure 3A shows that liposomes are formed from pure DPPC. This is consistent with the DRY-MARTINI model.[73] Similar to Lee and Pastor[33] (with DPPE-PEG), the liposome structure is also favored in PEG2.2 (Figure 3B). In PEG10.5 (Figure 3C), only bicelles are formed, whereas the PEG50 system (Figure 3D) produces slightly

DOI: 10.1021/acs.langmuir.8b03829
Langmuir 2019, 35, 3999−4010

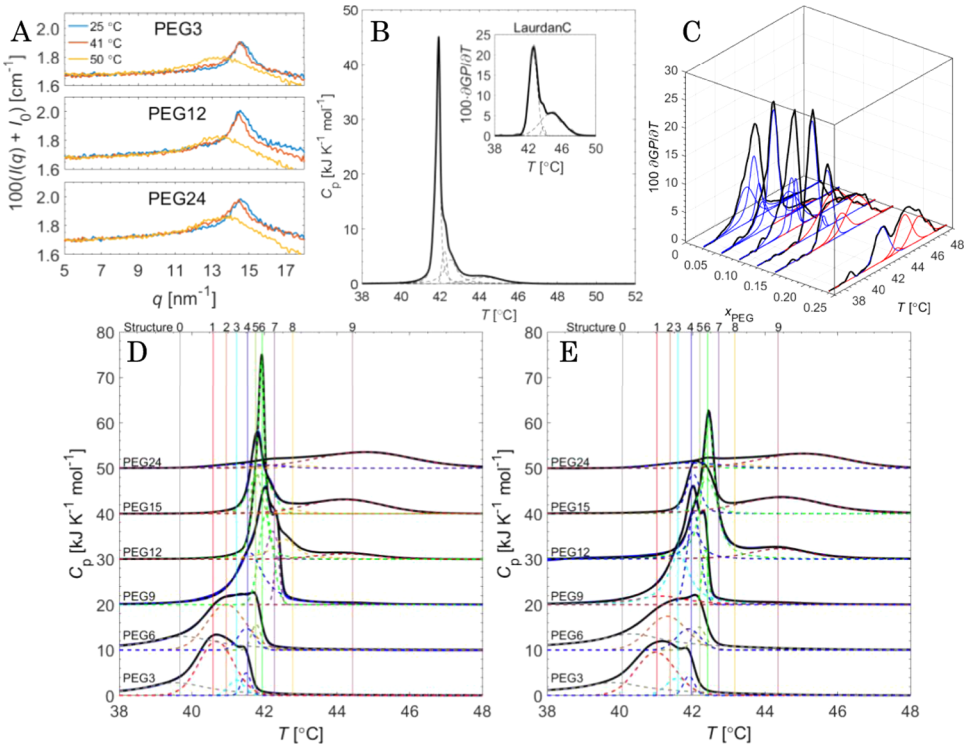

Figure 4. (A) WAXS intensity (I_0 is the average scattering intensity of water) vs scattering vector of PEG3, PEG12, and PEG24. (B) Deconvolutions (dashed lines) of the PEG12 sample measured with DSC and laurdanC (inset) (black lines). (C) LaurdanC GP differentials of PEGylated samples with color coding liposomal (blue) and "bicellar" (red). (D) DSC down-scan and (E) up-scan with colors marking the deconvoluted subgroups.

elongated micelles. Thus, the transition observed in the molecular modeling is in very good agreement with the cryo-TEM and SAXS results. In addition to larger simulations, Figure 3E shows a PEG10.5 bicelle of 1050 molecules. Here, the PEGylated lipids prefer the edge more likely than the bicelle face, in accordance with the SAXS result in Figure 2E and earlier computational works by Lee and Pastor[33] and Shinoda et al.,[35] who showed that the translocation decreases the line tension at the bicelle edge. This effect is also depicted in Figure 3F, where the density profile of DSPE lipids in bicelle (Figure 3E) is presented. These simulations represent systems with ca. 140 mM of lipids, which is 14-fold the experimental value in the equilibrium but realistic as a local concentration during the self-assembly. The concentration should not have a significant effect on the aggregate shape, because it is mainly controlled by molecular packing.

The simulations in Figure 3A–D contain 10 500 lipids. Due to the system size and finite simulation time, the formed aggregates are smaller than in the experiments.[82] For instance, the 2.2 mol % DSPE-PEG system (Figure 3B) produces liposomes with a mean radius of 7.5 nm, whereas cryo-TEM (Figure 1H) and SAXS analysis (Figure 2B) result in a radius closer to 35 nm. On the other hand, the simulation with 10.5 mol % DSPE-PEG (Figure 3C) leads to the formation of a set of bicelles with the largest ones between 9.5 and 11.5 nm in radius. These values are close to those obtained in the experiments. The PEG chain radius of gyration was 1.54 nm in all simulated samples. The value is in good agreement with the hydrodynamic radii obtained with SAXS (Figure 2D), especially as the radius of gyration calculated from the simulation does not encompass the hydration shell. Finally, in the simulations, the thickness of the bilayer corresponding to PEG3 is 5.0 ± 0.1 nm and increases for PEG11.1 to 5.2 ± 0.5 nm (see the Supporting Information). This trend is in line with the SAXS results, even though the SAXS fits are less sufficient in the high q region and the fitted head group is more involved with the water barrier than the simulations.

Thermal Analyses and the Phase Transition in the Lipid Bilayer. The structures of lipid bilayers showed no significant differences in the WAXS measurements of PEG3, PEG12, and PEG24 (Figure 4A, up-to-down), or in the samples shown in Figure S1. The lipid bilayer portrays near hexagonal packing or gel phase at 25 °C since the Bragg peak is found at ca. 14.5 nm^{-1} (blue line).[83] At 50 °C (orange line), the bilayer is in the fluid phase and only a broad peak is observed just below 14 nm^{-1}. At 41 °C (red line), DPPC is in the ripple phase and the Bragg peak is found at ca. 14.4 nm^{-1}. However, the overall shape is almost equal to that at 25 °C.

The downward DSC scan of a PEG12 sample and the corresponding laurdanC generalized polarization differential are shown in Figure 4B. As can be seen, the enthalpy can be deconvoluted to four contributions. Similarly, GP differentials (Figure 4C), downward (Figure 4D), and upward (Figure 4E) DSC peaks are composed of multiple peaks. The emergence of particulate subgroups stems mainly from the uneven PEGylation. The average melting temperature increases as a function of PEG fraction. This can be expected since pure DPPC bilayers melt at ca. 41 °C, whereas a DSPE bilayer undergoes a phase transition at ca. 74 °C.[84] The increase in the phase transition temperature is also connected with the decrease in the overall lateral pressure as the fatty acid chains of DPPC and DSPE-PEG become increasingly mismatched as the membrane enriches with DSPE-PEG.[85,86] In addition to the increase in the melting temperature as shown in Figure

DOI: 10.1021/acs.langmuir.8b03829
Langmuir 2019, 35, 3999–4010

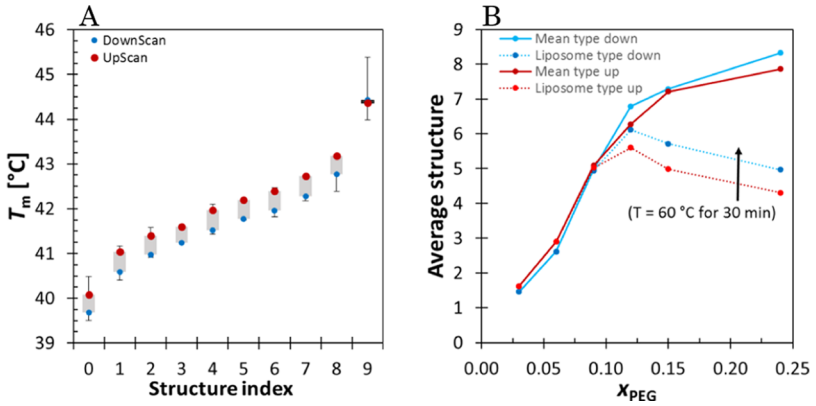

Figure 5. (A) Phase transition temperature from Figure 4D,E in the order of increasing temperature. (B) Average structure in the system vs x_{PEG}.

Table 1. Fraction of Bicelles in DSC Samples $x_{bicelle}^{DSC}$ Compared to Cryo-TEM ($x_{bicelle}^{TEM}$) and the Molar Enthalpy Change $\Delta H_{liposome}$ and $\Delta H_{bicelle}$

	$x_{bicelle}^{DSC}$ ($x_{bicelle}^{TEM}$) (%)					
x_{PEG}	0.09	0.12	0.15	0.24	$\Delta H_{liposome}$ (kJ mol^{-1})	$\Delta H_{bicelle}$ (kJ mol^{-1})
DSC up	1.72	19.97	55.45	77.64	29.49	12.51
DSC down	0.97	30.61	47.82	83.93	27.75	13.82
TEM	1.26 ± 0.14	17.38 ± 0.01	43.97 ± 0.85	83.44 ± 5.96		

4D,E, broad phase transition peaks, extending below 41 °C, are obtained in the liposomal samples. This is caused by the existence of smaller liposomes (<80 nm in diameter) with wide size distribution.[87]

The DSC deconvolution peaks were also color coded as displayed in Figure 4D,E. In the case of laurdanC measurements (Figure 4C), only liposomal (blue) and bicellar (red) phase transition peaks were extracted because the signal contains much less data points than the DSC measurements. Both the DSC upward and downward scans of the entire sample set exhibited ten deconvolution peaks. The phase transition temperatures are obviously not the same because the kinetics of freezing and melting are slightly different.

Figure 5A shows the deconvoluted subgroup peaks from Figure 4D,E with indexes from 0 to 9 in the order of their phase transition temperature. The error bars in Figure 5A mark the 95% confidence interval. The average structure in each sample is shown in Figure 5B. It shows that when the samples are kept for 30 min at 60 °C, the melting−freezing process is not completely reversible. Instead, a shift toward higher phase transition temperatures is observed in the PEG-rich samples, proving again that liposome structures in PEG12 and PEG15 are less stable than bicellar structures. The bicelle fraction was also calculated as $x_{bicelle}^{DSC} = \Delta H_{bicelle}/\Delta H_{tot}$, where the enthalpy of bicelles was calculated as the sum of the enthalpies of structures 8 and 9. This value is rather similar to that obtained with cryo-TEM (Table 1). In addition, the molar enthalpy change $\Delta H_{bicelle}$ and $\Delta H_{liposome}$ was calculated using $x_{bicelle}^{DSC}$ values.

The enthalpies in Table 1 represent only the main phase transition; the pre-phase transition was eliminated from the deconvolution for the sake of simplicity. Hence, liposomal enthalpies are ca. 2−4 kJ mol^{-1} lower than in the raw data. Table 1 shows a noticeable decrease in the average enthalpy when the system transforms from spherical liposomes to discoid bicelles.

Effect of Spontaneous Curvature. Preceding chapters imply that the onset of bicellation takes place between 9 and 12 mol % of PEG in the formulation. According to the laurdanC measurements, this transition is quite sharp. Comparison of $x_{bicelle}^{LC}$ (calculated from Figure 4C) with the logarithm of $x_{bicelle}^{TEM}$ shows a change in the slope at $x_{PEG}^{c} = 0.096$ (see Figure 6A,B). We interpret this point as the critical bicellation fraction (CBF).

LaurdanC measures electric polarity in its proximity.[88,89] Hence, its response in the bilayer is related to the area of the lipid−water boundary.[90,91] In the preliminary MD simulations, we found that laurdanC has lower mobility in the bilayer than the regular laurdan molecule because of its way of making hydrogen bonds with the lipid headgroups. This leads to assume that laurdanC resides in the facet of the bicelle rather than in the rims. This assumption is also supported by the fact that fraction $x_{bicelle}^{LC}$ does not approach unity when $x_{bicelle}^{TEM} \to 1$ (Figure 6A). Hence, we can derive an equation for the laurdanC GP fraction

$$x_{bicelle}^{LC} = \frac{GP_{bicelle}}{GP_{tot}} \approx \frac{A_{flat}}{A_{flat} + A_{curved}} = \frac{2(\eta - 1)^2}{2(\eta - 1)^2 + \pi(\eta - 1) + 1} \quad (13)$$

where A_{flat} and A_{curved} are the total areas of the flat and curved surfaces and $\eta = 1 + \frac{R_{flat}}{d_{HH}}$ is the aspect ratio. Here, the shape of the bicelle is the same as presented by Bergström,[52] with R_{flat} being the radius of the facet and d_{HH} = 4.4 nm being the approximate bilayer thickness from the lipid head group to another. When the measured $x_{bicelle}^{LC}$ are used to calculate η^{LC} with eq 13, an excellent correlation with η^{TEM} (determined from the micrographs) is obtained as shown in Figure 6C. LaurdanC measurement can thus determine the shape (aspect ratio) of the lipid system directly.

The limit radius $R_{flat\ limit} = d_{HH}(\eta_{limit} - 1)$ of bicelles can be obtained by calculating the aspect ratio of the limit $x_{bicelle}^{LC} \to 0.684$ (Figure 6A) with eq 13. With η^{LC}, this radius limit goes to $R_{flat\ limit}^{LC}$ = 16.2 nm, which is presumably the hydrodynamic

DOI: 10.1021/acs.langmuir.8b03829
Langmuir 2019, 35, 3999−4010

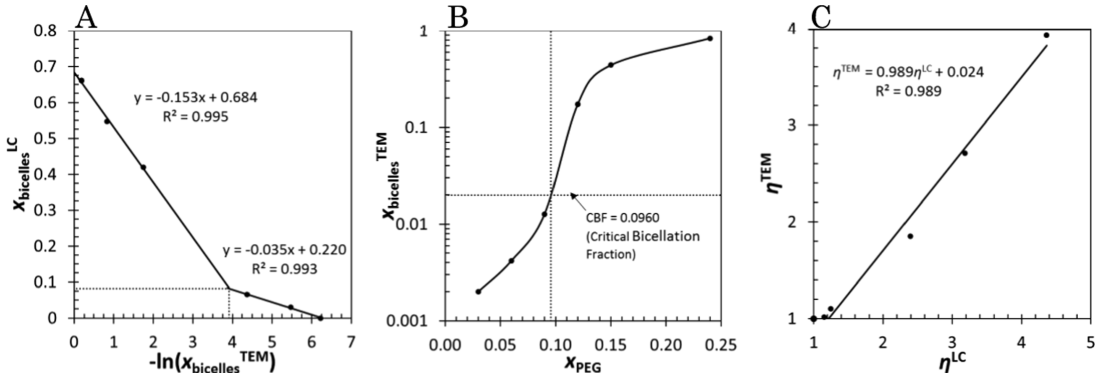

Figure 6. A) Log-linear relationship between $x_{\text{bicelle}}^{\text{TEM}}$ and $x_{\text{bicelle}}^{\text{LC}}$. The change in the slope occurs at CBF, which is converted to x_{PEG} in (B) (see the cross-section of the dotted lines in (A) and (B)). (C) Aspect ratio η^{LC} vs η^{TEM}. η^{LC} values are obtained from measured $x_{\text{bicelle}}^{\text{LC}}$ by using the eq 13.

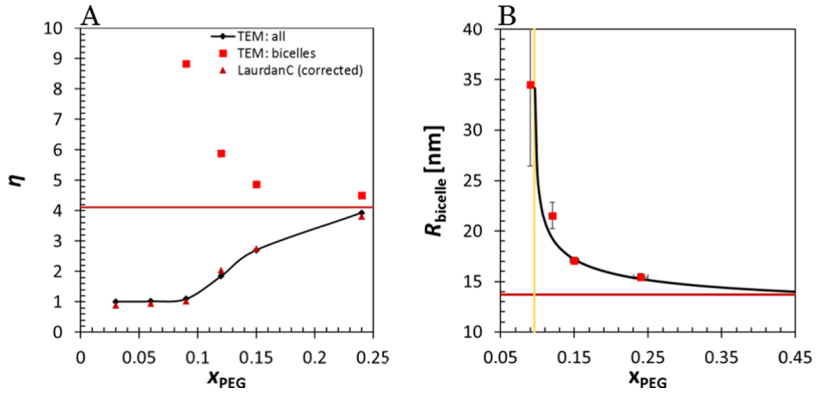

Figure 7. (A) Aspect ratio of bicelles and for the whole system in TEM (red squares and black diamonds) and the aspect ratio of the whole system with laurdanC (corrected to TEM scale, dark red triangles). The limit aspect ratio is shown as a red line. (B) The size of the bicelles, fitted with an empirical eq 14 based on CBF (light gold line) and the limit radius (red line).

radius. When the η^{LC} values are corrected to the TEM aspect ratio scale with the trend line in Figure 6C, an aspect ratio limit of 4.69 is reached (red line in Figure 7A), that is equivalent with the disc radius $R_{\text{flat limit}}^{\text{TEM}}$ = 13.7 nm (red line in Figure 7B). With the two critical parameters, CBF (or $x_{\text{PEG}}^{\text{c}}$) and $R_{\text{flat limit}}^{\text{TEM}}$, we can also set an empirical relationship for the bicelle radii as

$$\left(\frac{R_{\text{bicelle}}}{R_{\text{flat limit}}^{\text{TEM}}}\right)^{-6} = \frac{\langle A\rangle_{\text{DPPC}}}{\langle A\rangle_{\text{DSPE-PEG}}} \ln\frac{x_{\text{PEG}}}{x_{\text{PEG}}^{\text{c}}} \tag{14}$$

where $\langle A\rangle_{\text{DPPC}}$ = 52 Å^2 and $\langle A\rangle_{\text{DSPE-PEG}} \approx$ 91 Å^2. This fit is shown in Figure 7B.

The shape of a lipid particulate comes from the conditions of minimum curvature energy.[45,46] Thus, it connects the critical parameters $x_{\text{PEG}}^{\text{c}}$ and $R_{\text{flat limit}}^{\text{TEM}}$ in eq 14. The connection is evident by a simple continuum mechanics examination of the system energetics. The key contributor is the bending energy

$$H = \frac{1}{2}\kappa(K_1 + K_2 - K_0)^2 + \bar{\kappa}_{\text{G}}K_1K_2 \tag{15}$$

where κ is the bending modulus, $\bar{\kappa}_{\text{G}}$ is the Gaussian curvature modulus, K_1 and K_2 are the two principal total curvatures of the bilayer, and K_0 is the spontaneous total curvature. Together with the surface tension, minimizing the surface area, the bending contribution aims to minimize the difference $K_1 + K_2 - K_0$ throughout the bilayer. The surface stress can be written by combining eq 15 with the total curvature $K_{12} = K_1 + K_2$ and the surface tension γ

$$f = \frac{1}{2}\kappa(K_{12} - K_0)^2 + \gamma \tag{16}$$

Even though the terms $|\kappa|$ and $\bar{\kappa}_{\text{G}}$ are of the same magnitude in eq 15, the latter term has little effect on the shape ($\bar{\kappa}_{\text{G}}$ is more important when membrane fusion and fission are in question).[52,92] Hence, the Gaussian curvature contribution can be omitted. In addition, it should be noted that the spontaneous total curvature K_0 is double of the commonly used spontaneous curvature with the usual notations c_0 or H_0.[92] The minimum of eq 16 is the minimum of the free energy and therefore one can obtain a prediction for the shape transformation (see, e.g., ref 37).

Let us assume that the spontaneous total curvature of the mixture $K_{0,\text{mix}}$ follows simple additivity,[93] $K_{0,\text{mix}} = x_{\text{PEG}}K_{0,\text{DSPE-PEG}} + (1 - x_{\text{PEG}})K_{0,\text{DPPC}}$ and the surface tension is a constant. The transition from liposomes to bicelles occurs at the concentration in which the lipid mixture is capable of making the bicelle edge. This condition applies also to tubule-forming systems.[40,41,43,44] The transition occurs when the spontaneous total curvature matches the curvature $K_{12} = 1/d_{\text{HH}}$. We have used the value d_{HH} = 4.4(5) to minimize eq 16 at x_{PEG} = 0.096. The spontaneous total curvature values of individual lipids, $K_{0,\text{DPPC}}$ = 0.136 nm^{-1} [93] and = 1.06 nm^{-1},[94] can be extrapolated from the particle curvature vs particle radius plot, as shown in Figure 8A, where the lipid spontaneous curvatures are shown as black lines. The transition region is illustrated in Figure 8B, where the form of eq 16 ^{b} is added to the spontaneous total curvature of the

DOI: 10.1021/acs.langmuir.8b03829
Langmuir 2019, 35, 3999−4010

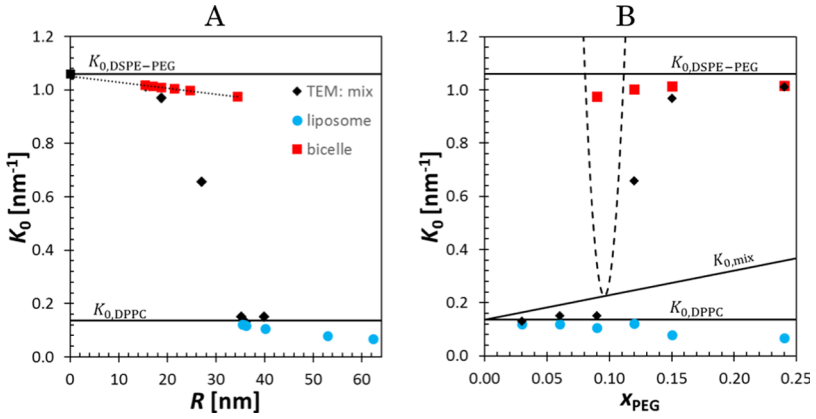

Figure 8. A) Mean curvature of liposomes (blue circles), bicelles (red squares), and system average (black diamond). (B) The observed mean curvature average (black triangles) as a function of PEG fraction. The critical bicelle fraction is found at the bending energy minimum at 9.6 mol % (with a bilayer thickness of ca. 4.45 nm). The bending energy is depicted as dashed parabola on the spontaneous curvature $K_{0,mix}$ line.

mixture (rising line). The bicelle transformation occurs at the minimum of the dashed parabola. Thereafter, the bicelles are decreased in size and eventually transform into spherical micelles. This transformation occurs when the spontaneous total curvature matches that of a sphere at $K_{12} = 4/d_{HH}$, which takes place at ca. 84 mol %. This is in perfect agreement with Ashok et al.,[4] who have reported a value of 85 mol % at the final transition point; their lipid, EPC, slightly differ in spontaneous curvature and thickness from DPPC.

CONCLUSIONS

PEGylation is the current state-of-the-art method to prolong circulation times of liposomal drug delivery systems in blood and in storage. Therefore, understanding the effects of PEGylation on the physicochemical properties of lipid particulates is important. In this paper, the effect of PEGylation in DPPC:DSPE-PEG(2000) systems was studied with cryo-TEM, DSC, SAXS, and fluorescence spectroscopy of laurdanC, as well as with molecular dynamics simulations. It was found that increasing the degree of PEGylation alters the fluidity of the bilayer and the shape of the lipid particulates. As demonstrated here, the shape-shift can be monitored with laurdanC. With the combination of laurdanC emission spectra and cryo-TEM, it was shown that the most visible transformation was from liposomes to bicelles when the fraction of the DSPE-PEG(2000) lipids reached the critical bicellation fraction (CBF), 9.6 mol %. We identified the greatest contribution to be the spontaneous curvature of the lipid components that is linked with the steric repulsion between PEG units in the lipid mixture. This means that lipids must relocate themselves to a region of curvature that matches their own.

The lipid curvature sets a limit to the sizes of units in the system. Liposome units have a limit size of ca. 30 nm which is characteristic to DPPC. Bicelle is characterized by the DSPE-PEG lipid that has an equivalent curvature of a micelle core 3.8 nm.[94] Bicelles are formed when the lipid mixture is capable of making bicelle edges with curvature $K_{12} = 1/d_{HH}$. The bicelle radius, in this case, was also effectively limited to the radius of ca. 14 nm.

Although the transformation to bicelles from liposomes is the most prominent phenomenon of the increased PEG fraction, we also found that other kinds of lipid particulates exist at the PEGylation fraction below bicellation. This is evident from the phase transition peak shifts of both DSC and laurdanC. Each melting temperature represents an individual PEG-layered lipid particulate. The driving force of the increasing melting temperature comes from the PEGylated lipids that were shown to affect membrane thickness and decrease the effective lateral pressure prior to bicellation.

The shift in the phase transition temperatures of spherical vesicles is connected to an increased bilayer thickness and improved shielding due to the PEG layer that evidently changes the surface pressure of the bilayer. This effect could be used to improve drug delivery systems. Since drug release occurs most effectively at the main phase transition temperature of the lipid, a mixture of liposomes with a range of phase transition temperatures can enable partial drug release by an accurate temperature control. This can be achieved with, e.g., photothermal agents.[14] Liposomes transform into bicelles when the spontaneous curvature of the mixture starts to favor the latter shape. The mechanism of action is a simple one. A lipid with a sizable polymer moiety on its head group has a positive curvature that controls the transformation. Hence, with a suitable polymer, it could be possible to trigger the transformation and activate the drug release.

ASSOCIATED CONTENT

Supporting Information

The Supporting Information is available free of charge on the ACS Publications website at DOI: 10.1021/acs.langmuir.8b03829.

Small/wide-angle X-ray scattering; molecular dynamics simulations: additional details; Matlab script for the Cryo-TEM analyses (PDF)

AUTHOR INFORMATION

Corresponding Author

*E-mail: lasse.murtomaki@aalto.fi.

ORCID

Lauri Viitala: 0000-0002-2734-372X
Luigi Gentile: 0000-0001-6854-2963
Maria Sammalkorpi: 0000-0002-9248-430X
Ulf Olsson: 0000-0003-2200-1605
Lasse Murtomäki: 0000-0001-7667-4325

Notes

The authors declare no competing financial interest.

DOI: 10.1021/acs.langmuir.8b03829
Langmuir 2019, 35, 3999−4010

■ ACKNOWLEDGMENTS

TEKES is acknowledged for funding via the "Light Activated Drug Delivery Systems" project (LADDS project). Academy of Finland is acknowledged for funding via grant 309324 (M.S.). Dr Dat Pham is acknowledged for the help in the DSC measurements. L.V. wishes to thank the Swedish-Finnish Cultural Foundation for a seven-day visiting grant to Lund University. This work made use of the Aalto University Nanomicroscopy Center (Aalto-NMC) premises. Computational resources from the CSC IT Center for Science, Finland, and RAMI RawMatTERS Finland Infrastructure are gratefully acknowledged.

■ ADDITIONAL NOTES

[a]From here on, the number after "PEG" indicates its mol % in the formulation.

[b]Bending modulus is replaced with $\kappa \rightarrow 2000$ nm to better illustrate the parabolic minimum.

■ REFERENCES

(1) Ali, M. H.; Moghaddam, B.; Kirby, D. J.; Mohammed, A. R.; Perrie, Y. The Role of Lipid Geometry in Designing Liposomes for the Solubilisation of Poorly Water Soluble Drugs. *Int. J. Pharm.* **2013**, *453*, 225−232.

(2) Lin, L.; Wang, X.; Guo, Y.; Ren, K.; Li, X.; Jing, L.; Yue, X.; Zhang, Q.; Dai, Z. Hybrid Bicelles as a pH-Sensitive Nanocarrier for Hydrophobic Drug Delivery. *RSC Adv.* **2016**, *6*, 79811−79821.

(3) Han, S.; Li, Z.; Zhu, J.; Han, K.; Zeng, Z.; Hong, W.; Li, W.; Jia, H.; Liu, Y.; Zhuo, R. Dual-pH Sensitive Charge-Reversal Polypeptide Micelles for Tumor-Triggered Targeting Uptake and Nuclear Drug Delivery. *Small* **2015**, *11*, 2543−2554.

(4) Ashok, B.; Arleth, L.; Hjelm, R. P.; Rubinstein, I.; Önyüksel, H. In Vitro Characterization of PEGylated Phospholipid Micelles for Improved Drug Solubilization: Effects of PEG Chain Length and PC Incorporation. *J. Pharm. Sci.* **2004**, *93*, 2476−2487.

(5) Ferreira, D. S.; Lopes, S.; Franco, M. S.; Oliveira, M. pH-Sensitive Liposomes for Drug Delivery in Cancer Treatment. *Ther. Delivery* **2013**, *4*, 1099−1123.

(6) Paasonen, L.; Romberg, B.; Storm, G.; Yliperttula, M.; Urtti, A.; Hennink, W. E. Temperature-Sensitive Poly(N-(2-Hydroxypropyl)-Methacrylamide Mono/Dilactate)-Coated Liposomes for Triggered Contents Release. *Bioconjugate Chem.* **2007**, *18*, 2131−2136.

(7) Paasonen, L.; Laaksonen, T.; Johans, C.; Yliperttula, M.; Kontturi, K.; Urtti, A. Gold Nanoparticles Enable Selective Light-Induced Contents Release from Liposomes. *J. Controlled Release* **2007**, *122*, 86−93.

(8) Paasonen, L.; Sipilä, T.; Subrizi, A.; Laurinmäki, P.; Butcher, S. J.; Rappolt, M.; Yaghmur, A.; Urtti, A.; Yliperttula, M. Gold-Embedded Photosensitive Liposomes for Drug Delivery: Triggering Mechanism and Intracellular Release. *J. Controlled Release* **2010**, *147*, 136−143.

(9) Lajunen, T.; Viitala, L.; Kontturi, L.; Laaksonen, T.; Liang, H.; Vuorimaa-Laukkanen, E.; Viitala, T.; Le Guével, X.; Yliperttula, M.; Murtomäki, L.; Urtti, A. Light Induced Cytosolic Drug Delivery from Liposomes with Gold Nanoparticles. *J. Controlled Release* **2015**, *203*, 85−98.

(10) Bouchaala, R.; Anton, N.; Anton, H.; Vandamme, T.; Vermot, J.; Smail, D.; Mély, Y.; Klymchenko, A. S. Light-Triggered Release from Dye-Loaded Fluorescent Lipid Nanocarriers in Vitro and in Vivo. *Colloids Surf., B* **2017**, *156*, 414−421.

(11) Troutman, T. S.; Leung, S. J.; Romanowski, M. Light-Induced Content Release from Plasmon-Resonant Liposomes. *Adv. Mater.* **2009**, *21*, 2334−2338.

(12) Lajunen, T.; Kontturi, L.; Viitala, L.; Manna, M.; Cramariuc, O.; Róg, T.; Bunker, A.; Róg, T.; Viitala, T.; Murtomäki, L.; Urtti, A. Indocyanine Green-Loaded Liposomes for Light-Triggered Drug Release. *Mol. Pharm.* **2016**, *13*, 2095−2107.

(13) Lajunen, T.; Nurmi, R.; Kontturi, L.; Viitala, L.; Yliperttula, M.; Murtomäki, L.; Urtti, A. Light Activated Liposomes: Functionality and Prospects in Ocular Drug Delivery. *J. Controlled Release* **2016**, *244*, 157−166.

(14) Viitala, L.; Pajari, S.; Lajunen, T.; Kontturi, L.; Laaksonen, T.; Kuosmanen, P.; Viitala, T.; Urtti, A.; Murtomäki, L. Photothermally Triggered Lipid Bilayer Phase Transition and Drug Release from Gold Nanorod and Indocyanine Green Encapsulated Liposomes. *Langmuir* **2016**, *32*, 4554−4563.

(15) Mura, S.; Nicolas, J.; Couvreur, P. Stimuli-Responsive Nanocarriers for Drug Delivery. *Nat. Mater.* **2013**, *12*, 991−1003.

(16) Jansen, M.; Blume, A. A Comparative Study of Diffusive and Osmotic Water Permeation Across Bilayers Composed of Phospholipids with Different Head Groups and Fatty Acyl Chains. *Biophys. J.* **1995**, *68*, 997−1008.

(17) Harashima, H.; Sakata, K.; Funato, K.; Kiwada, H. Enhanced Hepatic Uptake of Liposomes through Complement Activation Depending on the Size of Liposomes. *Pharm. Res.* **1994**, *11*, 402−406.

(18) Kari, O. K.; Rojalin, T.; Salmaso, S.; Barattin, M.; Jarva, H.; Meri, S.; Yliperttula, M.; Viitala, T.; Urtti, A. Multi-Parametric Surface Plasmon Resonance Platform for Studying Liposome-Serum Interactions and Protein Corona Formation. *Drug Delivery Transl. Res.* **2017**, *7*, 228−240.

(19) Klibanov, A. L.; Maruyama, K.; Torchilin, V. P.; Huang, L. Amphipathic Polyethyleneglycols Effectively Prolong the Circulation Time of Liposomes. *FEBS Lett.* **1990**, *268*, 235−237.

(20) Bunker, A.; Magarkar, A.; Viitala, T. Rational Design of Liposomal Drug Delivery Systems, a Review: Combined Experimental and Computational Studies of Lipid Membranes, Liposomes and their PEGylation. *Biochim. Biophys. Acta, Biomembr.* **2016**, *1858*, 2334−2352.

(21) Peracchia, M. T.; Vauthier, C.; Passirani, C.; Couvreur, P.; Labarre, D. Complement Consumption by Poly(Ethylene Glycol) in Different Conformations Chemically Coupled to Poly(Isobutyl 2-Cyanoacrylate) Nanoparticles. *Life Sci.* **1997**, *61*, 749−761.

(22) Barenholz, Y. Doxil—the First FDA-Approved Nano-Drug: Lessons Learned. *J. Controlled Release* **2012**, *160*, 117−134.

(23) Tirosh, O.; Barenholz, Y.; Katzhendler, J.; Priev, A. Hydration of Poly(ethylene glycol)-Grafted Liposomes. *Biophys. J.* **1998**, *74*, 1371−1379.

(24) Holland, J. W.; Hui, C.; Cullis, P. R.; Madden, T. D. Poly(ethylene glycol)-Lipid Conjugates Regulate the Calcium-Induced Fusion of Liposomes Composed of Phosphatidylethanolamine and Phosphatidylserine. *Biochemistry* **1996**, *35*, 2618−2624.

(25) Magarkar, A.; Karakas, E.; Stepniewski, M.; Róg, T.; Bunker, A. Molecular Dynamics Simulation of PEGylated Bilayer Interacting with Salt Ions: A Model of the Liposome Surface in the Bloodstream. *J. Phys. Chem. B* **2012**, *116*, 4212−4219.

(26) Dinç, C. Ö.; Kibarer, G.; Güner, A. Solubility Profiles of Poly(ethylene glycol)/Solvent Systems. II. Comparison of Thermodynamic Parameters from Viscosity Measurements. *J. Appl. Polym. Sci.* **2010**, *117*, 1100−1119.

(27) Furumoto, K.; Yokoe, J.; Ogawara, K.; Amano, S.; Takaguchi, M.; Higaki, K.; Kai, T.; Kimura, T. Effect of Coupling of Albumin Onto Surface of PEG Liposome on its in Vivo Disposition. *Int. J. Pharm.* **2007**, *329*, 110−116.

(28) Lee, H.; Larson, R. G. Adsorption of Plasma Proteins Onto PEGylated Lipid Bilayers: The Effect of PEG Size and Grafting Density. *Biomacromolecules* **2016**, *17*, 1757−1765.

(29) Lajunen, T.; Nurmi, R.; Wilbie, D.; Ruoslahti, T.; Johansson, N. G.; Korhonen, O.; Rog, T.; Bunker, A.; Ruponen, M.; Urtti, A. The Effect of Light Sensitizer Localization on the Stability of Indocyanine Green Liposomes. *J. Controlled Release* **2018**, *284*, 213−223.

(30) Lee, H.; de Vries, A. H.; Marrink, S.; Pastor, R. W. A Coarse-Grained Model for Polyethylene Oxide and Poly(ethylene glycol): Conformation and Hydrodynamics. *J. Phys. Chem. B* **2009**, *113*, 13186−13194.

DOI: 10.1021/acs.langmuir.8b03829
Langmuir 2019, 35, 3999−4010

(31) Rossi, G.; Fuchs, P.; Barnoud, J.; Monticelli, L. A Coarse-Grained MARTINI Model of Poly(ethylene glycol) and of Polyoxyethylene Alkyl Ether Surfactants. *J. Phys. Chem. B* **2012**, *116*, 14353−14362.
(32) Grunewald, F.; Rossi, G.; de Vries, A. H.; Marrink, S. J.; Monticelli, L. Transferable MARTINI Model of Poly(Ethylene Oxide). *J. Phys. Chem. B* **2018**, *122*, 7436−7449.
(33) Lee, H.; Pastor, R. W. Coarse-Grained Model for PEGylated Lipids: Effect of PEGylation on the Size and Shape of Self-Assembled Structures. *J. Phys. Chem. B* **2011**, *115*, 7830−7837.
(34) Yang, S.; Faller, R. Pressure and Surface Tension Control Self-Assembled Structures in Mixtures of Pegylated and Non-Pegylated Lipids. *Langmuir* **2012**, *28*, 2275−2280.
(35) Shinoda, W.; Discher, D. E.; Klein, M. L.; Loverde, S. M. Probing the Structure of PEGylated-Lipid Assemblies by Coarse-Grained Molecular Dynamics. *Soft Matter* **2013**, *9*, 11549−11556.
(36) Määttä, J.; Vierros, S.; Van Tassel, P. R.; Sammalkorpi, M. Size-Selective, Noncovalent Dispersion of Carbon Nanotubes by PEGylated Lipids: A Coarse-Grained Molecular Dynamics Study. *J. Chem. Eng. Data* **2014**, *59*, 3080−3089.
(37) Määttä, J.; Vierros, S.; Sammalkorpi, M. Controlling Carbon-Nanotube-Phospholipid Solubility by Curvature-Dependent Self-Assembly. *J. Phys. Chem. B* **2015**, *119*, 4020−4032.
(38) Vuorte, M.; Määttä, J.; Sammalkorpi, M. Simulations Study of Single Component and Mixed N-Alkyl-PEG Micelles. *J. Phys. Chem. B* **2018**, *122*, 4851−4860.
(39) Baekmark, T. R.; Pedersen, S.; Jørgensen, K.; Mouritsen, O. G. The Effects of Ethylene Oxide Containing Lipopolymers and Tri-Block Copolymers on Lipid Bilayers of Dipalmitoylphosphatidylcholine. *Biophys. J.* **1997**, *73*, 1479−1491.
(40) Edwards, K.; Johnsson, M.; Karlsson, G.; Silvander, M. Effect of Polyethyleneglycol-Phospholipids on Aggregate Structure in Preparations of Small Unilamellar Liposomes. *Biophys. J.* **1997**, *73*, 258−266.
(41) Johnsson, M.; Edwards, K. Liposomes, Disks, and Spherical Micelles: Aggregate Structure in Mixtures of Gel Phase Phosphatidylcholines and Poly(ethylene glycol)-Phospholipids. *Biophys. J.* **2003**, *85*, 3839−3847.
(42) Ickenstein, L. M.; Sandström, M. C.; Mayer, L. D.; Edwards, K. Effects of Phospholipid Hydrolysis on the Aggregate Structure in DPPC/DSPE-PEG 2000 Liposome Preparations After Gel to Liquid Crystalline Phase Transition. *Biochim. Biophys. Acta, Biomembr.* **2006**, *1758*, 171−180.
(43) Sandström, M. C.; Johansson, E.; Edwards, K. Influence of Preparation Path on the Formation of Discs and Threadlike Micelles in DSPE-PEG2000/Lipid Systems. *Biophys. Chem.* **2008**, *132*, 97−103.
(44) Arleth, L.; Ashok, B.; Onyuksel, H.; Thiyagarajan, P.; Jacob, J.; Hjelm, R. P. Detailed Structure of Hairy Mixed Micelles Formed by Phosphatidylcholine and PEGylated Phospholipids in Aqueous Media. *Langmuir* **2005**, *21*, 3279−3290.
(45) Helfrich, W. Elastic Properties of Lipid Bilayers: Theory and Possible Experiments. *Z. Naturforsch. C* **1973**, *28*, 693−703.
(46) Deuling, H.; Helfrich, W. The Curvature Elasticity of Fluid Membranes: A Catalogue of Vesicle Shapes. *J. Phys.* **1976**, *37*, 1335−1345.
(47) Marsh, D. Intrinsic Curvature in Normal and Inverted Lipid Structures and in Membranes. *Biophys. J.* **1996**, *70*, 2248−2255.
(48) Kunz, W.; Testard, F.; Zemb, T. Correspondence between Curvature, Packing Parameter, and Hydrophilicâ'Lipophilic Deviation Scales Around the Phase-Inversion Temperature. *Langmuir* **2009**, *25*, 112−115.
(49) Tanford, C. Micelle Shape and Size. *J. Phys. Chem.* **1972**, *76*, 3020−3024.
(50) Israelachvili, J. N.; Mitchell, D. J.; Ninham, B. W. Theory of Self-Assembly of Hydrocarbon Amphiphiles into Micelles and Bilayers. *J. Chem. Soc., Faraday Trans. 2* **1976**, *72*, 1525−1568.
(51) Langevin, D. Micelles and Microemulsions. *Annu. Rev. Phys. Chem* **1992**, *43*, 341−369.
(52) Bergström, L. M. Bending Energetics of Tablet-Shaped Micelles: A Novel Approach to Rationalize Micellar Systems. *ChemPhysChem* **2007**, *8*, 462−472.
(53) Cheniour, M.; Gueyrard, D.; Goekjian, P. G.; Granjon, T.; Marcillat, O. A Convenient and Versatile Synthesis of Laurdan-Like Fluorescent Membrane Probes: Characterization of their Fluorescence Properties. *RSC Adv.* **2016**, *6*, 5547−5557.
(54) Kuntsche, J.; Horst, J. C.; Bunjes, H. Cryogenic Transmission Electron Microscopy (Cryo-TEM) for Studying the Morphology of Colloidal Drug Delivery Systems. *Int. J. Pharm.* **2011**, *417*, 120−137.
(55) Iancu, C. V.; Tivol, W. F.; Schooler, J. B.; Dias, D. P.; Henderson, G. P.; Murphy, G. E.; Wright, E. R.; Li, Z.; Yu, Z.; Briegel, A.; et al. Electron Cryotomography Sample Preparation using the Vitrobot. *Nat. Protoc.* **2006**, *1*, 2813−2819.
(56) Ruzi, M. Voigt Line Shape Fit. https://se.mathworks.com/matlabcentral/fileexchange/57603-voigt-line-shape-fit (accessed May 21, 2017).
(57) Abrarov, S. M.; Quine, B. M. The Voigt/Complex Error Function. https://se.mathworks.com/matlabcentral/fileexchange/47801-the-voigt-complex-error-function--second-version (accessed May 21, 2017).
(58) Pedersen, J. S.; Gerstenberg, M. C. Scattering Form Factor of Block Copolymer Micelles. *Macromolecules* **1996**, *29*, 1363−1365.
(59) Pedersen, J. S. Analysis of Small-Angle Scattering Data from Colloids and Polymer Solutions: Modeling and Least-Squares Fitting. *Adv. Colloid Interface Sci.* **1997**, *70*, 171−210.
(60) Derici, L.; Ledger, S.; Mai, S.; Booth, C.; Hamley, I. W.; Pedersen, J. S. Micelles and Gels of Oxyethylene−oxybutylene Diblock Copolymers in Aqueous Solution: The Effect of Oxyethylene-Block Length. *Phys. Chem. Chem. Phys.* **1999**, *1*, 2773−2785.
(61) Pedersen, J. S. Form Factors of Block Copolymer Micelles with Spherical, Ellipsoidal and Cylindrical Cores. *J. Appl. Crystallogr.* **2000**, *33*, 637−640.
(62) Kučerka, N.; Kiselev, M. A.; Balgavý, P. Determination of Bilayer Thickness and Lipid Surface Area in Unilamellar Dimyristoylphosphatidylcholine Vesicles from Small-Angle Neutron Scattering Curves: A Comparison of Evaluation Methods. *Eur. Biophys. J.* **2004**, *33*, 328−334.
(63) Singh, D. *Small Angle Scatting Studies of Self Assembly in Lipid Mixtures*; The Johns Hopkins University, 2009.
(64) Arleth, L.; Vermehren, C. An Analytical Model for the Small-Angle Scattering of Poly(ethylene glycol)-Modified Liposomes. *J. Appl. Crystallogr.* **2010**, *43*, 1084−1091.
(65) Skar-Gislinge, N.; Arleth, L. Small-Angle Scattering from Phospholipid Nanodiscs: Derivation and Refinement of a Molecular Constrained Analytical Model Form Factor. *Phys. Chem. Chem. Phys.* **2011**, *13*, 3161−3170.
(66) Rayleigh, L. The Incidence of Light upon a Transparent Sphere of Dimensions Comparable with the Wave-Length. *Proc. R. Soc. A* **1910**, *84*, 25−46.
(67) Fournet, G. Scattering Functions for Geometrical Forms. *Bull. Soc. Fr. Mineral. Cristallogr.* **1951**, *74*, 39−113.
(68) Hammouda, B. Structure Factor for Starburst Dendrimers. *J. Polym. Sci., Part B: Polym. Phys.* **1992**, *30*, 1387−1390.
(69) Hammouda, B. SANS from Homogeneous Polymer Mixtures: A Unified Overview. In *Polymer Characteristics*; Springer, 1993; pp 87−133.
(70) Debye, P. Molecular-Weight Determination by Light Scattering. *J. Phys. Colloid Chem.* **1947**, *51*, 18−32.
(71) Marrink, S. J.; de Vries, A. H.; Mark, A. E. Coarse Grained Model for Semiquantitative Lipid Simulations. *J. Phys. Chem. B* **2004**, *108*, 750−760.
(72) Marrink, S. J.; Risselada, H. J.; Yefimov, S.; Tieleman, D. P.; De Vries, A. H. The MARTINI Force Field: Coarse Grained Model for Biomolecular Simulations. *J. Phys. Chem. B* **2007**, *111*, 7812−7824.
(73) Arnarez, C.; Uusitalo, J. J.; Masman, M. F.; Ingólfsson, H. I.; de Jong, D. H.; Melo, M. N.; Periole, X.; de Vries, A. H.; Marrink, S. J. Dry Martini, a Coarse-Grained Force Field for Lipid Membrane

DOI: 10.1021/acs.langmuir.8b03829
Langmuir 2019, 35, 3999−4010

Simulations with Implicit Solvent. *J. Chem. Theory Comput.* **2015**, *11*, 260−275.
(74) Pronk, S.; Páll, S.; Schulz, R.; Larsson, P.; Bjelkmar, P.; Apostolov, R.; Shirts, M. R.; Smith, J. C.; Kasson, P. M.; van der Spoel, D.; Hess, B.; Lindahl, E. GROMACS 4.5: A High-Throughput and Highly Parallel Open Source Molecular Simulation Toolkit. *Bioinformatics* **2013**, *29*, 845−854.
(75) Bussi, G.; Donadio, D.; Parrinello, M. Canonical Sampling through Velocity Rescaling. *J. Chem. Phys.* **2007**, *126*, No. 014101.
(76) de Jong, D. H.; Baoukina, S.; Ingólfsson, H. I.; Marrink, S. J. Martini Straight: Boosting Performance using a Shorter Cutoff and GPUs. *Comput. Phys. Commun.* **2016**, *199*, 1−7.
(77) Aslan, S.; Määttä, J.; Haznedaroglu, B. Z.; Goodman, J. P.; Pfefferle, L. D.; Elimelech, M.; Pauthe, E.; Sammalkorpi, M.; Van Tassel, P. R. Carbon Nanotube Bundling: Influence on Layer-by-Layer Assembly and Antimicrobial Activity. *Soft Matter* **2013**, *9*, 2136−2144.
(78) Almgren, M.; Edwards, K.; Karlsson, G. Cryo Transmission Electron Microscopy of Liposomes and Related Structures. *Colloids Surf., A* **2000**, *174*, 3−21.
(79) Pili, B.; Reddy, L. H.; Bourgaux, C.; Lepêtre-Mouelhi, S.; Desmaële, D.; Couvreur, P. Liposomal Squalenoyl-Gemcitabine: Formulation, Characterization and Anticancer Activity Evaluation. *Nanoscale* **2010**, *2*, 1521−1526.
(80) Bhat, R.; Timasheff, S. N. Steric Exclusion is the Principal Source of the Preferential Hydration of Proteins in the Presence of Poly(ethylene glycol). *Protein Sci.* **1992**, *1*, 1133−1143.
(81) Garbuzenko, O.; Barenholz, Y.; Priev, A. Effect of Grafted PEG on Liposome Size and on Compressibility and Packing of Lipid Bilayer. *Chem. Phys. Lipids* **2005**, *135*, 117−129.
(82) Sammalkorpi, M.; Karttunen, M.; Haataja, M. Structural Properties of Ionic Detergent Aggregates: A Large-Scale Molecular Dynamics Study of Sodium Dodecyl Sulfate. *J. Phys. Chem. B* **2007**, *111*, 11722−11733.
(83) Saveyn, P.; Van der Meeren, P.; Zackrisson, M.; Narayanan, T.; Olsson, U. Subgel Transition in Diluted Vesicular DODAB Dispersions. *Soft Matter* **2009**, *5*, 1735−1742.
(84) Kastantin, M.; Ananthanarayanan, B.; Karmali, P.; Ruoslahti, E.; Tirrell, M. Effect of the Lipid Chain Melting Transition on the Stability of DSPE-PEG(2000) Micelles. *Langmuir* **2009**, *25*, 7279−7286.
(85) Marsh, D.; Bartucci, R.; Sportelli, L. Lipid Membranes with Grafted Polymers: Physicochemical Aspects. *Biochim. Biophys. Acta, Biomembr.* **2003**, *1615*, 33−59.
(86) Pantusa, M.; Bartucci, R.; Marsh, D.; Sportelli, L. Shifts in Chain-Melting Transition Temperature of Liposomal Membranes by Polymer-Grafted Lipids. *Biochim. Biophys. Acta, Biomembr.* **2003**, *1614*, 165−170.
(87) Biltonen, R. L.; Lichtenberg, D. The use of Differential Scanning Calorimetry as a Tool to Characterize Liposome Preparations. *Chem. Phys. Lipids* **1993**, *64*, 129−142.
(88) Parasassi, T.; Krasnowska, E.; Bagatolli, L.; Gratton, E. Laurdan and Prodan as Polarity-Sensitive Fluorescent Membrane Probes. *J. Fluoresc.* **1998**, *8*, 365−373.
(89) Kawski, A.; Kukliński, B.; Bojarski, P.; Diehla, H. Ground and Excited State Dipole Moments of LAURDAN Determined from Solvatochromic and Thermochromic Shifts of Absorption and Fluorescence Spectra. *Z. Naturforsch., A* **2000**, *55*, 817−822.
(90) Vogel, V.; Möbius, D. Hydrated Polar Groups in Lipid Monolayers: Effective Local Dipole Moments and Dielectric Properties. *Thin Solid Films* **1988**, *159*, 73−81.
(91) Vogel, V.; Möbius, D. Local Surface Potentials and Electric Dipole Moments of Lipid Monolayers: Contributions of the Water/Lipid and the Lipid/Air Interfaces. *J. Colloid Interface Sci.* **1988**, *126*, 408−420.
(92) Deserno, M. Fluid Lipid Membranes: From Differential Geometry to Curvature Stresses. *Chem. Phys. Lipids* **2015**, *185*, 11−45.
(93) Kollmitzer, B.; Heftberger, P.; Rappolt, M.; Pabst, G. Monolayer Spontaneous Curvature of Raft-Forming Membrane Lipids. *Soft Matter* **2013**, *9*, 10877−10884.
(94) Vuković, L.; Khatib, F. A.; Drake, S. P.; Madriaga, A.; Brandenburg, K. S.; Král, P.; Onyuksel, H. Structure and Dynamics of Highly PEG-Ylated Sterically Stabilized Micelles in Aqueous Media. *J. Am. Chem. Soc.* **2011**, *133*, 13481−13488.

DOI: 10.1021/acs.langmuir.8b03829
Langmuir 2019, 35, 3999−4010